A&A 650, L15 (2021)
https://doi.org/10.1051/0004-6361/202141371

Astronomy & Astrophysics

LETTER TO THE EDITOR

Detection of deuterated methylcyanoacetylene, CH_2DC_3N, in TMC-1★

C. Cabezas[1], E. Roueff[2], B. Tercero[3,4], M. Agúndez[1], N. Marcelino[1], P. de Vicente[3], and J. Cernicharo[1]

[1] Grupo de Astrofísica Molecular, Instituto de Física Fundamental (IFF-CSIC), C/ Serrano 121, 28006 Madrid, Spain
e-mail: carlos.cabezas@csic.es; jose.cernicharo@csic.es
[2] LERMA, Observatoire de Paris, PSL Research University, CNRS, Sorbonne Universités, 92190 Meudon, France
[3] Observatorio Astronómico Nacional (IGN), C/ Alfonso XII, 3, 28014 Madrid, Spain
[4] Centro de Desarrollos Tecnológicos, Observatorio de Yebes (IGN), 19141 Yebes, Guadalajara, Spain

Received 22 May 2021 / Accepted 6 June 2021

ABSTRACT

We report the first detection in space of the single deuterated isotopologue of methylcyanoacetylene, CH_2DC_3N. A total of 15 rotational transitions, with J = 8–12 and K_a = 0 and 1, were identified for this species in TMC-1 in the 31.0–50.4 GHz range using the Yebes 40 m radio telescope. The observed frequencies were used to derive for the first time the spectroscopic parameters of this deuterated isotopologue. We derive a column density of $(8.0 \pm 0.4) \times 10^{10}$ cm^{-2}. The abundance ratio of CH_3C_3N to CH_2DC_3N is ∼22. We also theoretically computed the principal spectroscopic constants of ^{13}C isotopologues of CH_3C_3N and CH_3C_4H and those of the deuterated isotopologues of CH_3C_4H for which we could expect a similar degree of deuteration enhancement. However, we have not detected either CH_2DC_4H or CH_3C_4D, nor any ^{13}C isotopologues. The different observed deuterium ratios in TMC-1 are reasonably accounted for by a gas-phase chemical model where the low temperature conditions favour deuteron transfer through reactions with H_2D^+.

Key words. astrochemistry – ISM: molecules – ISM: individual objects: TMC-1 – line: identification – molecular data

1. Introduction

Deuterium fractionation is a well-known process in the dense interstellar medium that can occur both in the gas phase and on the surfaces of dust particles. This process allows deuterated isotopic species of interstellar molecules to reach abundances much higher than the D/H elemental abundance ratio (1.5×10^{-5} Linsky 2003). The high efficiency of deuterium fractionation allows deuterated species to achieve abundances as high as 30–40% relative to the parent species, as occurs with HDCS (Marcelino et al. 2005) and CH_2DOH (Parise et al. 2006). Hence, deuterated isotopologues of abundant interstellar molecules make a significant contribution to the spectral richness of line surveys. This makes the astronomical identification of these isotopologues of utmost importance, not only to gain knowledge on their molecular formation pathways or how deuterium fractionation works, but also to assign unidentified features in line surveys.

Very sensitive broadband line surveys of astronomical sources can now be achieved thanks to new technical developments in radio astronomy. These surveys have boosted the number of new molecular identifications in recent years because weak lines arising from low-abundance species and from low-dipole moment species can be now easily detected (Agúndez et al. 2021a; Cernicharo et al. 2021a,b,c). The negative counterpart of this high sensitivity is the huge number of new lines that populate the survey, including isotopologues and vibrationally excited states, in warm environments of well-known species. Hence, discovering spectral features of new molecules requires a previous detailed analysis of the spectral contribution of known species.

Methylcyanoacetylene, CH_3C_3N, also known as cyanopropyne or methylpropionitrile, has been detected with high abundance in the cold dark cloud TMC-1 (Broten et al. 1984) and more recently by Marcelino et al. (2021) using a high-sensitivity line survey on TMC-1 gathered with the Yebes 40 m radio telescope (see e.g., Cernicharo et al. 2021d). Hence, the deuterated isotopologues of CH_3C_3N are good candidates to be observed in this source using the same line survey. We have already detected other singly deuterated isotopologues of species such as CH_3CN, CH_3CCH, c-C_3H_2, C_4H, H_2C_4, H_2CCN, HC_3N, and HC_5N (Cabezas et al. 2021).

In this Letter we report the identification of spectral lines of the deuterated species CH_2DC_3N in TMC-1. Our search for this molecule is based on the change in the rotational parameters of CH_3C_3N produced by the H–D exchange, which have been obtained by ab initio calculations. The derived deuterium ratios are compared to an extended chemical model including the related deuterated compounds.

2. Observations

The Q-band observations of TMC-1 (α_{J2000} = 4^{h}41^{m}41.9^s and δ_{J2000} = +25°41′27.0″) described in this work were performed in several sessions between November 2019 and April 2021. They were carried out using a set of new receivers, built within the Nanocosmos project[1], and installed at the Yebes 40 m radio telescope.

★ Based on observations carried out with the Yebes 40 m telescope (projects 19A003, 20A014, and 20D15). The 40 m radiotelescope at Yebes Observatory is operated by the Spanish Geographic Institute (IGN, Ministerio de Transportes, Movilidad y Agenda Urbana).

[1] https://nanocosmos.iff.csic.es/

The Q-band receiver consists of two high-electron-mobility transitor cold amplifiers covering the 31.0–50.4 GHz band in the horizontal and vertical polarizations. The receiver temperature varies from 22 K at 32 GHz to 42 K at 50 GHz. The spectrometers formed by $2 \times 8 \times 2.5$ GHz fast Fourier transforms (FFTs) provide a spectral resolution of 38.15 kHz and cover the whole Q band in both polarizations. The receivers and the spectrometers are described in Tercero et al. (2021).

Different frequency coverages were observed, 31.08–49.52 GHz and 31.98–50.42 GHz, which permited us to check that no spurious ghosts were produced in the down-conversion chain when the signal coming from the receiver was downconverted to 1–19.5 GHz, and was then split into eight bands with a coverage of 2.5 GHz, each of which was analysed by the FFTs.

The observing procedure used was the frequency switching mode, with a frequency throw of 10 MHz or 8 MHz (see e.g., Cernicharo et al. 2021d,e,f). The intensity scale, or antenna temperature (T_A^*), was calibrated using two absorbers at different temperatures and the atmospheric transmission model ATM (Cernicharo 1985; Pardo et al. 2001). Calibration uncertainties of 10% were adopted, based on the observed repeatability of the line intensities between different observing runs. All data were analysed using the GILDAS package[2].

3. Results

The identification of most of the features from our TMC-1 Q-band line survey was done using the MADEX code (Cernicharo 2012) and the CDMS and JPL catalogues (Müller et al. 2005; Pickett et al. 1998). Nevertheless, many lines remain unidentified. Among these U lines we found a series of five lines with a harmonic relation 8:9:10:11:12 between them. This series of lines could be fitted using a Hamiltonian for a linear molecule obtaining accurate values for B and D constants: $B = 1989.428172 \pm 0.000610$ MHz and $D = 0.10950 \pm 0.00269$ kHz. However, a deeper inspection of the survey around the mentioned lines revealed the presence of two additional series of lines at higher and lower frequencies from the first series. The spectral pattern, taking into account all the lines, is easily recognizable as the typical a-type transition spectrum of a near-prolate molecule, with the sets of rotational transitions containing $J+1_{0,J+1} \leftarrow J_{0,J}$, $J+1_{1,J+1} \leftarrow J_{1,J}$, and $J+1_{1,J} \leftarrow J_{1,J-1}$ separated by $B + C$. All the observed lines, shown in Table 1 and Fig. 1, were analysed using an asymmetric rotor Hamiltonian in the FITWAT code (Cernicharo et al. 2018) to derive the rotational and centrifugal distortion constants shown in Table 2. With the available data we could not determine the A rotational constant, which was kept fixed to the ab initio value, as explained below.

The identification of the spectral carrier is first based on the following points: (i) the molecule is a closed-shell species without any appreciable fine or hyperfine interaction or large amplitude motion; (ii) the determined values for B and C constants indicate that the molecule is a very slightly asymmetric rotor, because B and C values are similar; and (iii) the $(B+C)/2$ value (1989.43 MHz, corresponding to the rotational constant of the close symmetric species) is smaller than that of H_2C_5 (2295.29 MHz), but larger than that of H_2C_6 (1344.72 MHz), which indicates that the molecule should contain four C atoms and one atom heavier than C. With these assumptions, we excluded species with four carbon atoms and a sulfur atom because they are too heavy. Species containing four carbon atoms and oxygen, like HC_4O (Kohguchi et al. 1994) and H_2C_4O (Brown et al. 1979), are rejected as candidates because they are too light (B = 2279.914 MHz and $(B + C)/2 = 2153.75$ MHz, respectively) and other species derived from them are too heavy or are open-shell species. Molecules with four carbon atoms and nitrogen could be good candidates. The HC_4N molecule (Tang et al. 1999) has a rotational constant $B = 2302.398$ MHz, and $(B+C)/2$ values for the cationic species HC_4NH^+ and $H_2C_4N^+$ in their $^1\Sigma$ electronic ground states have been calculated to be 2159.3 MHz and 2194.7 MHz, respectively (CCSD/cc-pVTZ level of theory; Cížek et al. 1969; Dunning 1989). The next member of this hydrogen addition progression is CH_3C_3N, whose rotational constant is 2065.74 MHz, very close to our $(B+C)/2$ value. This prompted us to think that the spectral carrier could be the deuterated isotopologue CH_2DC_3N, an asymmetric rotor, because the H–D interchange breaks the C_{3v} symmetry of CH_3C_3N.

We performed geometry optimization calculations for CH_3C_3N and CH_2DC_3N in order to estimate the isotopic shift on the rotational constants for the CH_3C_3N-CH_2DC_3N system.

Table 1. Observed line parameters for CH_2DC_3N in TMC-1.

$(J_{K_a,K_c})_u - (J_{K_a,K_c})_l$	ν_{obs} [a] (MHz)	$\int T_A^* dv$ [b] (mK km s^{-1})	Δv [c] (km s^{-1})	T_A^* (mK)
$8_{1,8} - 7_{1,7}$	31 797.891	2.08 ± 0.12	0.84 ± 0.15	2.3 ± 0.4
$8_{0,8} - 7_{0,7}$	31 830.626	2.76 ± 0.07	0.79 ± 0.11	3.3 ± 0.4
$8_{1,7} - 7_{1,6}$	31 862.950	1.39 ± 0.20	0.70 ± 0.12	1.9 ± 0.4
$9_{1,9} - 8_{1,8}$	35 772.575	1.67 ± 0.14	0.64 ± 0.11	2.5 ± 0.4
$9_{0,9} - 8_{0,8}$	35 809.389	3.11 ± 0.04	0.69 ± 0.06	4.3 ± 0.3
$9_{1,8} - 8_{1,7}$	35 845.744	1.31 ± 0.16	0.74 ± 0.14	3.1 ± 0.3
$10_{1,10} - 9_{1,9}$	39 747.236	0.73 ± 0.30	0.45 ± 0.15	1.6 ± 0.4
$10_{0,10} - 9_{0,9}$	39 788.132	2.66 ± 0.06	0.67 ± 0.07	3.8 ± 0.4
$10_{1,9} - 9_{1,8}$	39 828.533	1.07 ± 0.34	0.62 ± 0.16	1.6 ± 0.4
$11_{1,11} - 10_{1,10}$	43 721.867	1.45 ± 0.33	0.73 ± 0.32	1.9 ± 0.4
$11_{0,11} - 10_{0,10}$	43 766.845	2.11 ± 0.10	0.47 ± 0.09	4.2 ± 0.4
$11_{1,10} - 10_{1,9}$	43 811.297	1.77 ± 0.24	0.98 ± 0.35	1.7 ± 0.4
$12_{1,12} - 11_{1,11}$	47 696.518	0.86 ± 0.40	0.82 ± 0.20	2.1 ± 0.5
$12_{0,12} - 11_{0,11}$	47 745.519	1.91 ± 0.10	0.46 ± 0.06	3.9 ± 0.5
$12_{1,11} - 11_{1,10}$	47 794.026	0.83 ± 0.46	0.45 ± 0.11	1.7 ± 0.5

Notes. [a]Observed frequencies towards TMC-1 for which we adopted a v_{LSR} of 5.83 km s^{-1} (Cernicharo et al. 2020a,b,c). The frequency uncertainty 10 kHz. [b]Integrated line intensity in mK km s^{-1}. [c]Line width at half intensity derived by fitting a Gaussian function to the observed line profile (in km s^{-1}).

Table 2. Observationally derived and theoretical spectroscopic parameters (in MHz) for CH_2DC_3N.

Constant	Space [a]	Ab initio [b]
A	120120.70 [c]	120120.70
B	1993.493107(593)	1993.53
C	1985.363112(657)	1985.74
Δ_J	9.107(230) 10^{-5}	–
Δ_{JK}	1.4767(249)10^{-2}	–
rms [d]	13.6	–
J_{min}/J_{max}	8/12	–
K_{min}/K_{max}	0/1	–
$N^{(e)}$	15	–

Notes. [a]Fit to the lines of CH_2DC_3N observed in TMC-1. [b]CCSD/cc-pVTZ level of theory. Scaled values using as reference CH_3C_3N; see text. [c]Fixed to the calculated value. [d]The standard deviation of the fit in kHz. [e]Number of lines included in the fit.

[2] http://www.iram.fr/IRAMFR/GILDAS

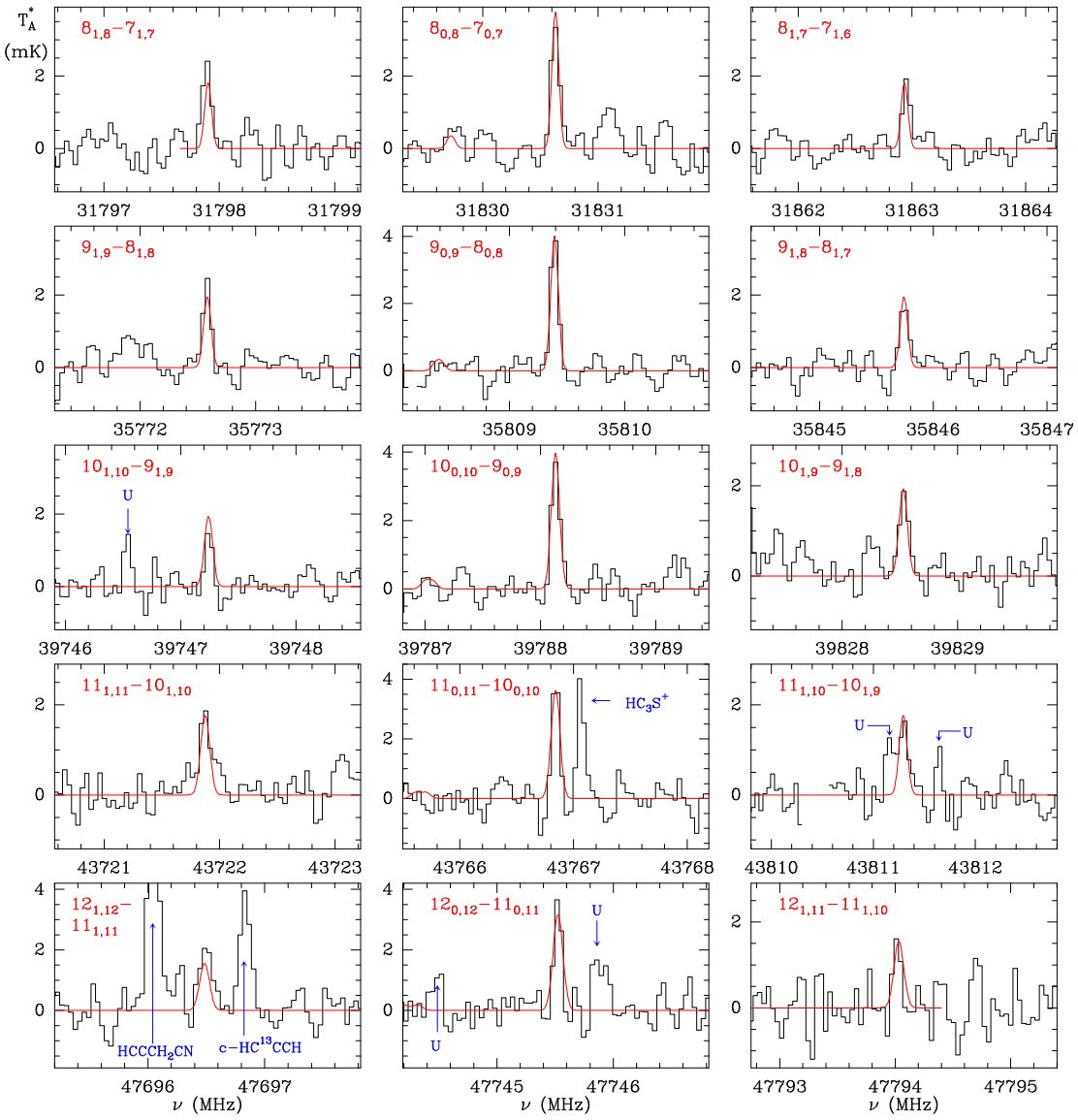

Fig. 1. Observed lines of CH_2DC_3N in TMC-1 in the 31.0–50.4 GHz range. Frequencies and line parameters are given in Table 1. Quantum numbers for the observed transitions are indicated in each panel. The red line shows the synthetic spectrum computed for a rotational temperature of 8 K and a column density of 8×10^{10} cm^{-2} (see text). The additional components seen in the synthetic spectrum close to the $K_a = 0$ components are the $K_a = 2$ rotational transitions. Blanked channels correspond to negative features created in the folding of the frequency switching data. The label '*U*' corresponds to features above 4σ.

Using the ratio of experimental to theoretical values is the most common method of predicting the expected experimental rotational constants for an isotopic species of a given molecule when the rotational constants for its parent species are known. Hence, we employed the CCSD/cc-pVTZ level of theory (Cížek et al. 1969; Dunning 1989), which reproduces well the B rotational constant for CH_3C_3N, 2058.0 MHz versus 2065.74 MHz. The theoretical values for the rotational constants of CH_2DC_3N were then scaled using the experimental/theoretical ratio obtained from CH_3C_3N, and the results are shown in Table 2. As can be seen, the predicted values for CH_2DC_3N perfectly match those derived from our fit, which allows us to conclude that the spectral carrier of our lines is CH_2DC_3N. It should be noted that the calculations provide the equilibrium values for the rotational constants (A_e, B_e and C_e), while the experimental values are the ground state rotational constants (A_0, B_0, and C_0). Even though the equilibrium rotational constants differ slightly from the ground state constants, we can assume similar discrepancies for CH_3C_3N and CH_2DC_3N, and thus that the estimated constants for CH_2DC_3N are essentially unaffected.

Methyldiacetylene (CH_3C_4H) is 7.5 times more abundant than, and lines have similar intensities to, CH_3C_3N (Marcelino et al. 2021; Cernicharo et al. 2021c). Hence, it is straightforward to think that spectral signatures of the deuterated species of CH_3C_4H could also be detected in our line survey. We followed the same strategy used for CH_2DC_3N to predict the transition frequencies of CH_2DC_4H. Laboratory values are available for CH_3C_4D (Heath et al. 1955). We carried out geometry optimization calculations for CH_3C_4H. The rotational constants obtained for CH_2DC_4H are shown in Table 3. We found only two lines at the predicted transition frequencies corresponding to $8_{0,8}$–$7_{0,7}$ and $9_{0,9}$–$8_{0,8}$ with intensities of ~1 mK. Other lines predicted in the frequency range of the line survey are below the present sensitivity. We consider that the deuterated isotopologue of CH_3C_4H is not detected so far (see below). The deuteration of this species is discussed in the following section.

Table 3. Predicted spectroscopic constants (in MHz) for isotopic species of CH_3C_3N and CH_3C_4H.

Species	B
$^{13}CH_3CCCN$	2010.51
$CH_3\ ^{13}CCCN$	2054.75
$CH_3C^{13}CCN$	2065.71
$CH_3CC^{13}CN$	2048.72
$CH_3CCC^{15}N$	2011.56
$^{13}CH_3CCCCH$	1982.60
$CH_3\ ^{13}CCCCH$	2025.34
$CH_3C^{13}CCCH$	2035.71 [(b)]
$CH_3CC^{13}CCH$	2018.90
$CH_3CCC^{13}CH$	1980.28
$CH_2DCCCCH$ [(a)]	A = 120899.40
	B = 1965.96
	C = 1958.41

Notes. For all the ^{13}C and ^{15}N species the A value can be assumed for the corresponding parent species, CH_3C_3N or CH_3C_4H, 158 099.0 and 159 140.0 MHz, respectively. [(a)]A, B, and C constants are provided due to the C_s symmetry of this species. [(b)]For this isotopologue laboratory data are available (Cazzoli et al. 2008). The experimental rotational constant B is 2035.67752 MHz.

Considering the intensity of the CH_3C_3N and CH_3C_4H lines in our line survey, we expected to observe the ^{13}C isotopologues as well. The frequency transitions for these species were predicted using the rotational constants from Table 3, which were obtained using the same procedure employed for the CH_2DC_3N isotopic species. However, we could not find spectral signatures for any of these species around the predicted frequencies.

The column density of CH_2DC_3N was derived from a rotational diagram analysis of the observed intensities. We assumed a source of uniform brightness with a radius of 40″ (Fossé et al. 2001). We derive $T_r = 8 \pm 0.5$ K and $N(CH_2DC_3N) = (8.0 \pm 0.4) \times 10^{10}$ cm^{-2}. As shown in Fig. 1, the agreement between the synthetic spectrum and the observations is excellent. The column density is not very sensitive to the adopted value of the rotational temperature between 6 and 10 K. For the normal isotopologue Marcelino et al. (2021) derived a rotational temperature for the A and E species of 6.7 ± 0.2 K and of 8.2 ± 0.6 K, respectively. They derived a total column density for CH_3C_3N of $(1.74 \pm 0.1) \times 10^{12}$ cm^{-2}. Hence, the CH_3C_3N/CH_2DC_3N abundance ratio is 22 ± 2.

The column density of CH_3C_4H has been derived by Cernicharo et al. (2021c) to be $(1.30 \pm 0.04) \times 10^{13}$ cm^{-2}. Assuming the same rotational temperature for CH_2DC_4H as for the main isotopologue (Cernicharo et al. 2021c), we derive a 3σ upper limit to its column density of 3.7×10^{11} cm^{-2}. Therefore, the CH_3C_4H-to-CH_2DC_4H abundance ratio is $\geq$35 (3σ). For the deuterated species CH_3C_4D, for which laboratory spectroscopy is available (Heath et al. 1955), we derive a 3σ upper limit to its column density of 9×10^{10} cm^{-2}. Hence, $N(CH_3C_4H)/N(CH_3C_4D) \geq 144$.

4. Chemical modelling

We further investigate the chemical processes leading to deuterium insertion in methylcyanoacetylene and methyldiacetylene by extending our previous study on H_2CCN and HDCCN (Cabezas et al. 2021). We only consider gas-phase mechanisms that allow quantitative predictions based on some experimental measurements and theoretical studies. The chemistry of the different C_4H_3N and C_5H_4 isomers has been discussed recently in Cernicharo et al. (2021c) and Marcelino et al. (2021), respectively, in relation with their detection in TMC-1. These two chemical families are tightly linked to the chemistry of methylacetylene, CH_3CCH, and its isomer allene, CH_2CCH_2:

$$\begin{aligned} CN + CH_3CCH &\rightarrow CH_3C_3N + H,\\ &\rightarrow HCN + CH_2CCH,\\ &\rightarrow HC_3N + CH_3;\\ C_2H + CH_3CCH &\rightarrow CH_3C_4H + H,\\ &\rightarrow H_2CCCHCCH + H, \end{aligned}$$

whereas

$$\begin{aligned} CN + CH_2CCH_2 &\rightarrow CH_2CCHCN + H,\\ &\rightarrow HCCCH_2CN + H;\\ C_2H + CH_2CCH_2 &\rightarrow CH_3C_4H + H,\\ &\rightarrow H_2CCCHCCH + H. \end{aligned}$$

Considering the deuterated analogues of these reactions introduces diverse questions, for example whether the CN reactions proceed without changing the methyl radical or lead to some scrambling of the hydrogen atoms in a quasi-stationary intermediate followed by different reaction channels. The first assumption would lead to the reactions

$$CN + CH_2DCCH \rightarrow CH_2DC_3N + H, \quad (1)$$
$$CN + CH_3CCD \rightarrow CH_3C_3N + D, \quad (2)$$

whereas the second option would introduce an additional reaction channel:

$$CN + CH_2DCCH \rightarrow CH_3C_3N + D, \quad (3)$$
$$CN + CH_3CCD \rightarrow CH_2DC_3N + H. \quad (4)$$

The case of the reactions involving C_2H (C_2D) is even more uncertain as an additional H(D) atom is involved, which leads to a complementary reaction channel:

$$C_2D + CH_3CCH \rightarrow CH_3C_4H + D, \quad (5)$$
$$\rightarrow CH_3C_4D + H, \quad (6)$$
$$\rightarrow CH_2DC_4H + H; \quad (7)$$
$$C_2H + CH_2DCCH \rightarrow CH_2DC_4H + H, \quad (8)$$
$$\rightarrow CH_3C_4D + H, \quad (9)$$
$$\rightarrow CH_3C_4H + D. \quad (10)$$

Similar questions arise in the deuteration mechanisms involving deuteron transfer initiated by reactions with abundant deuterated molecular ions such as H_2D^+ and DCO^+. As an example, the products of the $H_2D^+ + CH_3C_3N$ reaction could be $CH_3C_3ND^+ + H_2$, if the reaction proceeds directly, or also $CH_2DC_3NH^+ + H_2$, if an intermediate complex is formed[3] The following step in forming deuterated methylcyanoacetylene entails dissociative recombination of the molecular ion, where an additional question arises on the branching ratios of the reaction $CH_2DC_3NH^+ + e^- \rightarrow CH_2DC_3N + H$ and/or $\rightarrow CH_3C_3N + D$. These few examples show the multiple issues that emerge when analysing the potential chemical processes at work. We considered two different approaches. In case A we assume that the

[3] The channel $CH_3C_3NH^+ + HD$ is present in both cases as well.

Table 4. Deuteration enhancement in TMC-1 for detected molecules compared to our gas-phase chemical model.

Molecule	Observations TMC-1	Model A no scrambling	Model B full scrambling
CH_3C_3N/CH_2DC_3N	22 [(a)]	75.8	31.4
CH_3CN/CH_2DCN	11 [(b)]	15.0	15.0
$H_2CCN/HDCCN$	20 [(b)]	23.6	23.6
HC_3N/DC_3N	62 [(c)]	54.9	54.5
HNCCC/DNCCC	43 [(c)]	34.6	34.5
HCCNC/DCCNC	30 [(c)]	27.2	27.1
HC_5N/DC_5N [(b)]	82 [(c)]	23.3	23.3
$c\text{-}C_3H_2/c\text{-}C_3HD$	27 [(b)]	45.5	45.4
C_4H/C_4D	118 [(b)]	55.5	55.3
H_2C_4/HDC_4	83 [(b)]	49.5	49.4
CH_3CCH/CH_3CCD	49 [(b)]	257	264
CH_3CCH/CH_2DCCH	10 [(b)]	76	76
CH_3C_4H/CH_2DC_4H	≥35 [(d)]	59	20
CH_3C_4H/CH_3C_4D	≥144 [(d)]	136	55

Notes. [(a)]This work. [(b)]Cabezas et al. (2021). [(c)]Cernicharo et al. (2020a). [(d)]3σ upper limit.

methyl radical and its deuterated form keep their structure (e.g., as in reactions 1, 2, 5, 6, 8), whereas case B involves a scrambling of the H and D atoms followed by the formation of the different products (e.g., as in reactions 3, 4, 7, 9, 10). These hypotheses are implemented in a chemical model including 320 species and more than 9000 gas-phase reactions built from previous studies (Cabezas et al. 2021; Agúndez et al. 2021b). We display in Table 4 the corresponding steady-state ratios obtained in a model adapted to TMC-1 conditions, $n(H_2) = 4 \times 10^4$ cm^{-3}, $T = 10$ K, $\zeta = 1.3 \times 10^{-17}$ s^{-1}, as in Cabezas et al. (2021)[4]. We first note the significant sensitivity of the deuterium ratio for CH_3C_3N and CH_3C_4H to the reactivity assumptions. A low deuterium ratio, close to the observed value of CH_3C_3N, is favoured in the full scrambling approximation. The upper limits found for CH_3C_4H/CH_2DC_4H and CH_3C_4H/CH_3C_4D, on the other hand, are better reproduced when reactions 5, 6, and 8 are the only channels in the C_2H (C_2D) reactions. Whereas the other observed deuterium ratios are reasonably reproduced within a factor of 2, a significant discrepancy is still obtained for methylacetylene, CH_3CCH, as already noted in Cabezas et al. (2021) and Agúndez et al. (2021b). This feature arises because the reaction of CH_3CCH with H_3^+ (and supposedly H_2D^+) leads to the break up of CH_3CCH into $c\text{-}C_3H_3^+$ and $l\text{-}C_3H_3^+$ ($c\text{-}C_3H_2D^+$ and $l\text{-}C_3H_2D^+$) rather than to $C_3H_5^+$ or $C_3H_4D^+$ ($CH_3CCH_2^+$, $CH_2DCCH_2^+$, CH_3CCHD^+), as found in the experimental study of Milligan et al. (2002). We did not try to include additional deuterium exchange reactions, in the absence of any theoretical or experimental information.

We conclude this section by acknowledging the possible gas-phase deuteration mechanisms of cyanomethylacetylene mediated by deuteron transfer reactions with species such as H_2D^+ and DCO^+, among other deuterated cations in low-temperature conditions, but point out the substantial uncertainties involved in the different possible reactions, so that a detailed comparison between observations and chemical modeling appears elusive. A theoretical analysis of the intermolecular interaction potentials involved in the approach of the different reactants would help to validate the various reaction mechanisms.

[4] The elemental values (i.e., $O/H = 8 \times 10^{-6}$, $C/O = 0.75$, $N/O = 0.5$) correspond to a carbon-rich environment.

5. Conclusions

We have detected and unambiguously identified CH_2DC_3N, a new deuterated compound, in TMC-1 thanks to highly sensitive space observations of 15 different transitions and to the associated theoretical considerations and quantum mechanical calculations. Spectroscopic constants are also provided for that compound and the ^{13}C and ^{15}N substitutes, which should help to study those species in the laboratory as well. The observed deuterium fractions are further compared to a gas-phase model, which, despite significant uncertainties, accounts within a factor of two for the different values, except for CH_3CCH. Further experimental or theoretical studies are welcome.

Acknowledgements. We thank ERC for funding through grant ERC-2013-Syg-610256-NANOCOSMOS. The Spanish authors thank Ministerio de Ciencia e Innovación for funding support through project AYA2016-75066-C2-1-P, PID2019-106235GB-I00 and PID2019-107115GB-C21/AEI/10.13039/501100011033. MA thanks Ministerio de Ciencia e Innovación for grant RyC-2014-16277. ER acknowledges the support of the Programme National 'Physique et Chimie du Milieu Interstellaire' (PCMI) of CNRS/INSU with INC/INP co-funded by CEA and CNES. Several kinetic data we used have been taken from the online databases KIDA (Wakelam et al. 2012, http://kida.obs.u-bordeaux1.fr) and UMIST2012 (McElroy et al. 2013, http://udfa.ajmarkwick.net).

References

Agúndez, M., Cabezas, C., Tercero, B., et al. 2021a, A&A, 647, L10
Agúndez, M., Roueff, E., Cabezas, C., et al. 2021b, A&A, 649, A171
Broten, N. W., MacLeod, J. M., Avery, L. W., et al. 1984, ApJ, 276, L25
Brown, R. D., Brown, R. F. C., Eastwood, F. W., et al. 1979, J. Am. Chem. Soc., 101, 4705
Cabezas, C., Endo, Y., Roueff, E., et al. 2021, A&A, 646, L1
Cazzoli, G., Cludi, L., Contento, M., & Puzzarini, C. 2008, J. Mol. Spectrosc., 251, 229
Cernicharo, J. 1985, Internal IRAM report (Granada: IRAM)
Cernicharo, J. 2012, in European Conference on Laboratory Astrophysics, eds. C. Stehlé, C. Joblin, & L. d'Hendecourt, EAS Publ. Ser., 58, 251
Cernicharo, J., Guélin, M., Agúndez, M., et al. 2018, A&A, 618, A4
Cernicharo, J., Marcelino, N., Agúndez, M., et al. 2020a, A&A, 642, L17
Cernicharo, J., Marcelino, N., Pardo, J. R., et al. 2020b, A&A, 641, L9
Cernicharo, J., Marcelino, N., Agúndez, M., et al. 2020c, A&A, 642, L8
Cernicharo, J., Cabezas, C., Agúndez, M., et al. 2021a, A&A, 648, L3
Cernicharo, J., Agúndez, M., Cabezas, C., et al. 2021b, A&A, 647, L2
Cernicharo, J., Cabezas, C., Agúndez, M., et al. 2021c, A&A, 647, L3
Cernicharo, J., Agúndez, M., Cabezas, C., et al. 2021d, A&A, 649, L15
Cernicharo, J., Cabezas, C., Endo, Y., et al. 2021e, A&A, 646, L3
Cernicharo, J., Cabezas, C., Bailleux, S., et al. 2021f, A&A, 646, L7
Cížek, J. 1969, in Advances in Chemical Physics, ed. P. C. Hariharan (New York: Wiley Interscience), 14, 35
Dunning, T. H. 1989, J. Chem. Phys., 90, 1007
Fossé, D., Cernicharo, J., Gerin, M., & Cox, P. 2001, ApJ, 552, 168
Heath, G. A., Thomas, L. F., Sherrard, E. I., & Sheridan, J. 1955, Faraday Soc. Disc., 19, 38
Hickson, K. B., Wakelam, V., & Loison, J. C. 2016, Mol. Astrophys., 3, 1
Kohguchi, H., Ohshima, Y., & Endo, Y. 1994, J. Chem. Phys., 101, 6463
Linsky, J. L. 2003, Space Sci. Rev., 106, 49
Marcelino, N., Cernicharo, J., Roueff, E., et al. 2005, ApJ, 620, 308
Marcelino, N., Tercero, B. N., Agúndez, M., & Cernicharo, J. 2021, A&A, 646, L9
McElroy, D., Walsh, C., Markwick, A. J., et al. 2013, A&A, 550, A36
Milligan, D. B., Wilson, P. F., Freeman, C. G., et al. 2002, J. Phys. Chem. A, 106, 9745
Müller, H. S. P., Schlöder, F., Stutzki, J., & Winnewisser, G. 2005, J. Mol. Struct., 742, 215
Parise, B., Ceccarelli, C., Tielens, A. G. G. M., et al. 2006, A&A, 453, 949
Tang, J., Sumiyoshi, Y., & Endo, Y. 1999, Chem. Phys. Lett., 315, 69
Tercero, F., López-Pérez, J. A., Gallego, J. D., et al. 2021, A&A, 645, A37
Pardo, J. R., Cernicharo, J., & Serabyn, E. 2001, IEEE Trans. Antennas Propag., 49, 12
Pickett, H. M., Poynter, R. L., Cohen, E. A., et al. 1998, J. Quant. Spectr. Rad. Transfer, 60, 883
Wakelam, V., Loison, J.-C., Herbst, E., et al. 2012, ApJS, 199, 21